Letters

Deadbeat Control of Dual Active Bridge Converters With Adaptive Noise Resistance Ability

Dehao Kong, *Member, IEEE*, Tianxu Cao, *Student Member, IEEE*, Ralph Kennel, *Senior Member, IEEE*, and Marcelo Lobo Heldwein, *Senior Member, IEEE*

***Abstract*—Although deadbeat control offers excellent dynamic performance for dual active bridge (DAB) converters with relatively simple computations, it is sensitive to sampling noise, which degrades system performance and even leads to instability. Existing approaches based on digital filters induce higher computational burden and alter the system pole locations affecting the inherent characteristics of deadbeat-controlled DABs. Therefore, this letter proposes a novel deadbeat control method with adaptive noise resistance ability for DABs. Instead of digital filters, an adaptive attenuation coefficient is used to efficiently and adaptively mitigate the impact of noises, using a simple structure. Combing with the compensation term derived from the system model, it introduces no steady-state error and preserves the original closed-loop pole locations, thereby maximally retaining the essential features of deadbeat control. Experimental results verify the effectiveness and superiority of the proposed method.**

***Index Terms*—Deadbeat control, dual active bridge (DAB) converter, noise resistance.**

I. Introduction

OWING to its merits, such as high power density, wide range of voltage gain, and high controllability, the dual active bridge (DAB) converter is widely used in energy storage systems, microgrids, and related applications [1].

To enhance the dynamic performance of DABs' output port, many control methods based on advanced controllers have been proposed. A feedback linearization is used in [2] to cancel the nonlinear terms in the model, improving the dynamic speed. However, the parameters tuning is a tedious trial and error process. Sliding mode control (SMC) is also an alternative employed in [3], but the well-known chattering issues around the sliding surface is challenging. Although employing integral or higher order SMC can address this issue, the associated complexity correspondingly increases [4]. In [5] and [6], model predictive control is used to increase the response speed while minimizing the current stress and circulating power by its cost functions. Nevertheless, the computational burden is a challenge if the computation resource is limited.

Among them, deadbeat control is a promising alternative due to its fast response speed, less calculation, and fixed switching frequency [7]. Given the high-frequency operation and simple control structure (first-order system) of DABs, these features render deadbeat control an appropriate control strategy for the voltage regulation.

However, deadbeat voltage control is highly sensitive to various noises due to its high bandwidth and the adopted model structure. Such noises typically consist of switching noise, quantization noise (analog-to-digital process and pulse width modulation), and measurement noise [8]. Due to the presence of such noises, deadbeat control may suffer from severe chattering, leading to significant oscillations in the transformer current. This reduces the lifespan of converter components, causes electromagnetic interference issues, and degrades the overall control performance. In severe cases, system failure may occur as a result of overheating or controller instability. More critically, the severity of this issue increases with the rise of switching frequency (see analysis in Section II), which aligns with the prevailing trend toward smaller footprint.

To address this issue, sampling multiple times within a switching cycle, along with the corresponding data processing, is effective [9], [10]. However, it places higher demands on high-speed, parallel-execution hardware. A more practical solution is to adopt advanced digital filters [11], [12], [13]. However, this introduces a tradeoff between filtering strength and phase response, which may change the closed-loop characteristic and lead to low-frequency oscillations. This issue is particularly critical for deadbeat-controlled DAB converters, which are highly sensitive to measurement noise. Furthermore, the involved multiple coefficients make the tuning process complex and time-consuming.

More crucially, the involved additional control loop moves the system poles away from the origin, deviating from the basic principle of deadbeat control. In discrete systems, the core objective of deadbeat control is to place all closed-loop poles at the origin, thereby achieving finite-time convergence of the system states, which is called "dead-beat." Displaced poles may deteriorate the response speed and impose oscillations in

Received 3 September 2025; revised 3 November 2025; accepted 21 December 2025. Date of publication 24 December 2025; date of current version 25 February 2026. *(Corresponding author: Tianxu Cao.)*

The authors are with the Chair of High-Power Converter Systems, Technical University of Munich, 80333 Munich, Germany (e-mail: dehao.kong@tum.de; tianxu.cao@tum.de; ralph.kennel@tum.de; marcelo.heldwein@tum.de).

Color versions of one or more figures in this article are available at https://doi.org/10.1109/TPEL.2025.3648175.

Digital Object Identifier 10.1109/TPEL.2025.3648175

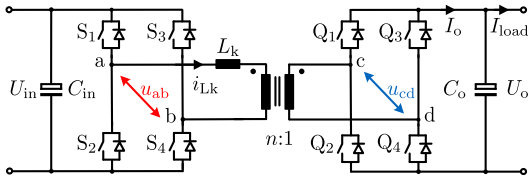

Fig. 1. Simplified topology of DABs.

the system. Therefore, a method that efficiently mitigates the impact of noises with simple tuning process, while maintaining the closed-loop poles at the origin, is of significance.

Thus, this letter proposes a novel deadbeat control method with an adaptive attenuation coefficient. First, the mechanism of noise impact is analyzed. Based on this, an attenuation coefficient with a compensation term is introduced, which practically and efficiently mitigates the noises without altering the closed-loop characteristic. Moreover, to cope with unpredictable noise environments, this coefficient is endowed with adaptive capability to ensure stable operation under varying conditions. Furthermore, a theoretical system analysis demonstrates that this method introduces no steady-state error and preserves the closed-loop pole positions. Lastly, the effectiveness of the proposed method is validated experimentally.

II. Impact of Noises on Control System

A. Impact of Output-Voltage Sampling Noise

Fig. 1 shows the topology of DABs. In discrete systems, the dynamic equation of its output port can be derived as

$$U_{\mathrm{o}}[k+1] = U_{\mathrm{o}}[k] + \frac{T_{\mathrm{s}}}{C_{\mathrm{o}}}(I_{\mathrm{o}}[k] - I_{\mathrm{load}}[k]) \tag{1}$$

where C_{o} and U_{o} are the output capacitor and voltage, respectively, I_{o} and I_{load} are the output current and load current, respectively, and T_{s} is the sampling period.

The time delay effect in a real digital system should be considered and compensated by a one-step ahead estimation method, thereby the discrete model for sampling time $t = k+2$ at $t = k$ can be derived as

$$U_{\mathrm{o}}[k+2] = U_{\mathrm{o}}[k+1] + \frac{T_{\mathrm{s}}}{C_{\mathrm{o}}}(I_{\mathrm{o}}[k+1] - I_{\mathrm{load}}[k+1]). \tag{2}$$

The deadbeat control of DABs generates the output current that allows the real voltage to exactly track the reference in the ideal case. Considering the influence of sampling noises, its control law can be calculated by

$$I_{\mathrm{o}}[k+1] = \frac{C_{\mathrm{o}}}{T_{\mathrm{s}}}(U_{\mathrm{o}}^{*} - U_{\mathrm{o}}[k+1] + \Delta u_{\mathrm{noi}}^{\mathrm{o}}) + I_{\mathrm{load}}[k] \tag{3}$$

where U_{o}^{*} is the reference, $U_{\mathrm{o}}[k+1]$ is obtained by (1), $I_{\mathrm{load}}[k] = I_{\mathrm{load}}[k+1]$ is assumed, and $I_{\mathrm{o}}[k+1]$ is used to produce the shift angles. For example, in the single-phase shift (SPS) modulation, the shift angle is $D = (1 - \sqrt{1 - \frac{8L_{\mathrm{k}}I_{\mathrm{o}}}{T_{\mathrm{s}}U_{\mathrm{in}}}})/2$, where L_{k} is the leakage inductance and U_{in} is the input voltage. In other multiple-phase shift modulations, the similar processes of modulation can be found in [1].

As shown in (3), inevitable noise $\Delta u_{\mathrm{noi}}^{\mathrm{o}}$ is introduced by the sampling process of $U_{\mathrm{o}}[k]$, which in turn affects the generation of

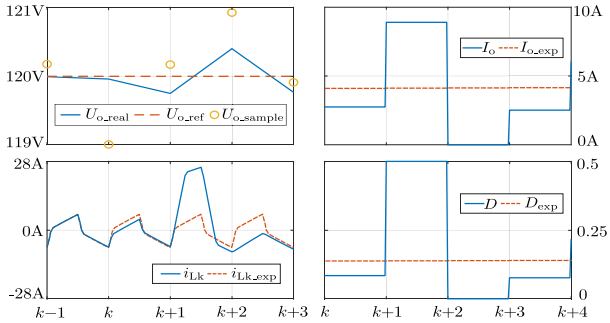

Fig. 2. Impact of $\Delta u_{\mathrm{noi}}^{\mathrm{o}}$ on the system.

$I_{\mathrm{o}}[k+1]$. It is reasonable to summarize these multiple regular noises, i.e., switching noise, quantization noise, and the measurement noise, to a zero-mean Gaussian white noise process, since such noises are, in general, broadband, uncorrelated, and exhibit random characteristics [14]. Moreover, by invoking the three-sigma (3σ) rule associated with Gaussian distributions, it can be inferred that approximately 99.7% of the noise values are confined within the range of $\pm 3\sigma$, where σ denotes the standard deviation [15].

Due to the presence of $\Delta u_{\mathrm{noi}}^{\mathrm{o}}$, the first term of (3) frequently varies between positive and negative values (it was expected to remain closely centered around zero), inducing significant chattering to $I_{\mathrm{o}}[k+1]$ and $D[k+1]$. This issue becomes particularly pronounced under light-load conditions (i.e., I_{load} is small) and at high switching frequencies (i.e., T_{s} is small), because the first term of (3) constitutes a more significant portion. As the noise level reaches a certain threshold, severe fluctuations may cause the entirety of $I_{\mathrm{o}}[k+1]$ (also $D[k+1]$) to toggle abruptly between positive and negative values. Besides $I_{\mathrm{o}}[k+1]$, given the peak transformer current as

$$I_{\mathrm{p}}[k+1] = \frac{U_{\mathrm{in}}T_{\mathrm{s}}}{4L_{\mathrm{k}}}(1 - m + 2mD[k+1]) \tag{4}$$

where $m = U_{\mathrm{o}}/U_{\mathrm{in}}$ is the voltage ratio, it is obvious that the transformer current is significantly affected as well. Such fluctuations in I_{o} and I_{p} induce audible noise from the converter, increased thermal stress, and even instability.

This phenomenon can be demonstrated by Fig. 2, where a noise signal with $\sigma = 0.25$ is injected (99.7% of the noise samples lie within ± 0.75 V). The sampled voltage contaminated with noise $U_{\mathrm{o\_sample}}$ fluctuates around the actual voltage, which causes the output current I_{o} and the phase shift angle D in the subsequent cycle to deviate sharply from their expected values ($I_{\mathrm{o\_exp}}$ and D_{exp}). This, in turn, induces oscillations and current spikes in the transformer current i_{Lk}, thereby further aggravating the chattering of the output voltage.

B. Comparative Analysis

In fact, apart from the output-voltage sampling noise $\Delta u_{\mathrm{noi}}^{\mathrm{o}}$, the input-voltage sampling noise $\Delta u_{\mathrm{noi}}^{\mathrm{in}}$ affects the system as well, introduced by the sampling process of $U_{\mathrm{in}}[k]$. This sampling process happens during the calculation of shift angle,

TABLE I
SPECIFICATIONS AND PARAMETERS OF PROTOTYPE

Parameter	Symbol	Value
Input voltage	U_{in}	150 V
Output voltage	U_{o}	120 V
Ratio of transformer	n	1
Leakage inductor	L_{k}	105 μH
Output capacitor	C_{o}	300 μF
Switching frequency	f_{s}	20k Hz

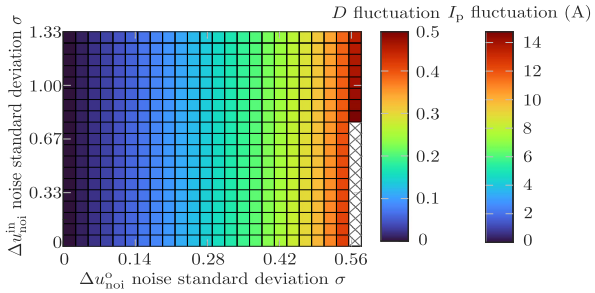

Fig. 3. Impacts comparison of $\Delta u^{\text{o}}_{\text{noi}}$ and $\Delta u^{\text{in}}_{\text{noi}}$.

which is shown in (5), taking the SPS as an example

$$D[k+1] = \frac{1}{2} - \frac{\sqrt{1 - \frac{8L_{\text{k}}I_{\text{o}}[k+1]}{T_{\text{s}}(U_{\text{in}}[k]+\Delta u^{\text{in}}_{\text{noi}})}}}{2}. \tag{5}$$

Overall, $\Delta u^{\text{o}}_{\text{noi}}$ influences the system via (3), while $\Delta u^{\text{in}}_{\text{noi}}$ influences the system via (5). In (3), due to the small difference between U^*_{o} and $U_{\text{o}}[k+1]$, the magnitude of $\Delta u^{\text{o}}_{\text{noi}}$ is a dominant factor, and is amplified by $\frac{C_{\text{o}}}{T_{\text{s}}}$, thereby exerting a substantial effect on the values of $I_{\text{o}}[k+1]$ and $D[k+1]$. Conversely, in (5), $\Delta u^{\text{in}}_{\text{noi}}$ appears only as an additional term and is much smaller. Meanwhile, the numerator and denominator of the fractional term under the square root are comparable. Consequently, $\Delta u^{\text{in}}_{\text{noi}}$ has only a limited influence on $D[k+1]$.

This can be further validated by numerically comparing the fluctuations. The results are obtained by defining the fluctuations of D and I_{p} as the difference between the one calculated by (3)–(5) and the one calculated by ideal sampling conditions, and using the parameters, as shown in Table I. The results are given in Fig. 3, where the color encodes the magnitude of fluctuations, with colorless regions indicating the invalid zone of shift angle. As can be seen, the impact of $\Delta u^{\text{in}}_{\text{noi}}$ induces a much smaller influence to D and I_{p}, compared with the impact of $\Delta u^{\text{o}}_{\text{noi}}$. Hence, the tiny impact of $\Delta u^{\text{in}}_{\text{noi}}$ can be ignored.

III. Deadbeat Control With Adaptive Noise Resistance Ability

A. Control Algorithm

To address the issue of sampling noise, a deadbeat controller with adaptive noise resistance ability is proposed. Instead of the digital filter, it maintains the poles at the origin and induces no steady-state errors, while employing a simpler structure.

According to the analysis above, the mechanism of the chattering lies in the existence of $\Delta u^{\text{o}}_{\text{noi}}$, which causes the first term of (3) to vary between positive and negative values, thereby affecting its overall value. Hence, an adaptive attenuation coefficient α, defined as $\alpha \in (0,1] \subset \mathbb{R}$, can be set, yielding (3) in the form of

$$I_{\text{o}}[k+1] = \frac{\alpha[k]C_{\text{o}}}{T_{\text{s}}}(U^*_{\text{o}} - U_{\text{o}}[k+1] + \Delta u^{\text{o}}_{\text{noi}}) + I_{\text{load}}[k]. \tag{6}$$

By introducing α, the robustness against noise is improved due to the reduced contribution of the first term in (6). As a result, the calculated $I_{\text{o}}[k+1]$ becomes more smooth and stable, since the first term tends to remain closely around zero.

In addition, to adapt the attenuation coefficient to the noise intensity, it can be expressed as

$$\alpha[k] = \min\left(\max\left(\frac{1}{1+\gamma\sigma_n[k]}, \alpha_{\min}\right), 1\right) \tag{7}$$

where the second and third terms, i.e., $\alpha_{\min}$ and 1, are the top and bottom limitations of attenuation coefficient, respectively. $\alpha_{\min} \in (0,1)$ is designed by considering the possible maximum on-site noise level and the tolerable noise-induced oscillation (refer to Fig. 5). $\sigma_n[k]$ is the noise intensity, which can be defined as

$$\sigma_n[k] = (1-\beta)\sigma_n[k-1] + \beta|\nu[k]| \tag{8}$$

where β is the smooth coefficient, and $\nu[k]$ is the measured noise that can be defined as $U^*_{\text{o}} - U_{\text{o}}[k]$. β can be tuned according to a low-pass filter. $\gamma > 0$ in (7) is used to adjust the sensitivity to noise variation. Its design needs an offline prior estimation that considers the possible maximum noise and the possible result calculated from (8). Therefore, defining the offline prior estimated result of (8) as σ_{est}, and given by the value of $\alpha_{\min}$, γ can be calculated by

$$\gamma = \frac{1-\alpha_{\min}}{\alpha_{\min}\sigma_{\text{est}}}. \tag{9}$$

Of course, the specific value may require lightly manual tuning in practice. In this case, α is able to be adjusted to deal with real-time noise variations.

However, it is obvious that such an attenuation coefficient will degrade both steady-state and transient performances, because the controller becomes less responsive to errors as a tradeoff for enhanced noise-resistant ability. This can be further validated by examining the system sensitivity. Specifically, applying (6) into the plant model (2) and considering Δu_{noi} as part of $U_{\text{o}}[k]$ for derivation simplicity leads to

$$\begin{aligned} U^a_{\text{o}}[k+2] = {} & (1-\alpha)U_{\text{o}}[k] + \alpha U^*_{\text{o}} \\ & + \frac{T_{\text{s}}}{C_{\text{o}}}(1-\alpha)(I_{\text{o}}[k] - I_{\text{load}}[k]) \\ & + \frac{T_{\text{s}}}{C_{\text{o}}}(I_{\text{load}}[k] - I_{\text{load}}[k+1]) \end{aligned} \tag{10}$$

where U^a_{o} is the actual value of state variable. As can be seen, it does not output an expected voltage, compared to the normal value, as shown in (14).

Therefore, an additional compensation term $\mathcal{A}$ should be added into (10), forcing (10) to be the normal value. Clearly, according to (6) and (10), $\mathcal{A}$ should be

$$\mathcal{A} = (1-\alpha)(U^*_{\text{o}} - U_{\text{o}}[k] - \frac{T_{\text{s}}}{C_{\text{o}}}(I_{\text{o}}[k] - I_{\text{load}}[k]))$$

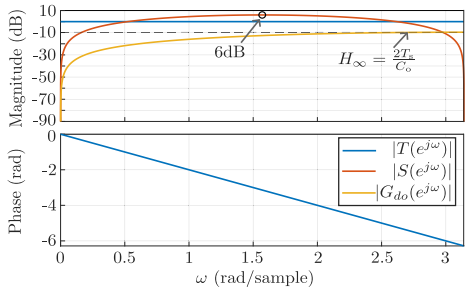

Fig. 4. System frequency-domain analysis.

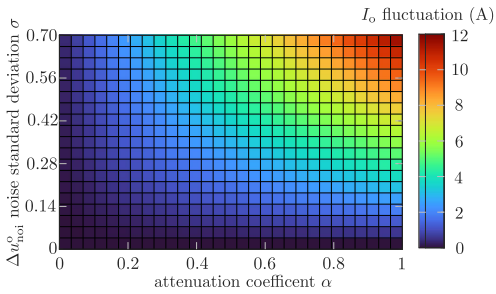

Fig. 5. Impact of α and $\Delta u^{o}_{\text{noi}}$ on output current fluctuation.

$$= \frac{T_s}{C_o}\left(\frac{1}{\alpha} - 1\right)(I_o[k+1] - I_{\text{load}}[k]). \tag{11}$$

That is to say, the DAB needs to additionally output a voltage illustrated in (11), by providing increased current.

Thus, following with the calculated result in (6), the revised control law can be assigned a new value as

$$I_o[k+1] := \mathcal{B} \tag{12}$$

where

$$\mathcal{B} = I_o[k+1] + (1-\alpha)(I_o[k+1] - I_{\text{load}}[k]). \tag{13}$$

Note that $I_o[k+1]$ in (13) is calculated by (6), and the value of final control law $I_o[k+1]$ in (12) is assigned by $\mathcal{B}$.

B. System Analysis and Evaluation

Similarly, the new actual value of output voltage can be derived by applying the final control law [see (6) and (12)] into the plant model (2), which is

$$U_o^a[k+2] = U_o^* + \frac{T_s}{C_o}(I_{\text{load}}[k] - I_{\text{load}}[k+1]). \tag{14}$$

Clearly, none of the coefficients associated with the noise resistance are present. Moreover, the behavior of the control system can be further evaluated by analyzing its steady-state and transient performances.

As for the influence on the steady-state performance, it is reasonable to assume that $U_o^a[k+2] = U_o^a[\infty]$ and $I_{\text{load}}[k] = I_{\text{load}}[k+1] = I_{\text{load}}[\infty]$ under the steady state, if the system does not change its operation point. Therefore, (15) can be deduced from (14), which is

$$U_o^a[\infty] = U_o^*. \tag{15}$$

It is obvious that the system regulated by the revised control law does not bring in any steady-state tracking error.

Regarding the influence on the transient performance, it can be testified by the discrete-time control theory analysis with z-transformation. In this case, considering the load current in (14) as a disturbance, the transfer function between the output voltage and the reference can be derived as

$$\frac{U_o^a[z]}{U_o^*[z]} = \frac{1}{z^2} \tag{16}$$

where the poles of the system are located at origin. This is also the basic principle and object of deadbeat control. In discrete-time control theory, a system is deemed stable if and only if all of its poles lie strictly within the unit circle, i.e., $|z| < 1$ [16]. Building on this, the closer the poles are to the origin, the faster the system responds, until they reach the origin, where the system achieves theoretical deadbeat performance.

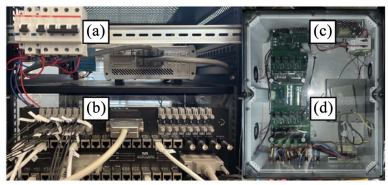

Fig. 6. DAB prototype for test. (a) dSPACE real-time control system. (b) Signal interface. (c) H-bridges. (d) Transformer.

This can be further analyzed in frequency-domain. Mapping the closed-loop transfer function (16) onto the unit circle gives $G_{\text{cl}}(e^{j\omega}) = e^{-j2\omega}$, $|G_{\text{cl}}| = 1$, and $\angle G_{\text{cl}} = -2\omega$. Thus, given the complementary sensitivity $T(e^{j\omega}) = G_{\text{cl}}(e^{j\omega})$, $|T(e^{j\omega})| = 1$, and $\angle T(e^{j\omega}) = -2\omega$ are obtained, corresponding to the definition of deadbeat control, i.e., the magnitude is unity across the entire frequency band, with a pure two-sample delay, and without gain peaking. Fig. 4 describes this case. Hence, it does not introduce frequency-domain resonance or overshoot amplification. Combining with the closed-loop poles located at $z = 0$, the system is considered as internal stability.

Moreover, given the sensitivity $S(z) = 1 - T(z) = 1 - z^{-2}$, $S(1) = 0$, implying zero steady-state error to constant references and complete rejection of constant (low-frequency) load disturbances at the output. The curve is drawn in Fig. 4. By using $z = e^{j\omega}$, its magnitude response can be expressed as $|S(e^{j\omega})| = |1 - e^{-j2\omega}| = 2|\sin\omega|$. Hence, several information can be obtained from this equation and Fig. 4 as follows.

1) When $\omega \to 0$ or $\omega \to \pi$, $|S| \to 0$ (magnitude response$\to -\infty$), which aligning with the meaning of $S(1) = 0$.

2) $|S(e^{j\omega})|$ reaches its maximum at $\omega = \pi/2$, with a single modest peak of 2 (6 dB), and remains bounded elsewhere.

3) Together with $T(e^{j\omega}) = e^{-j2\omega}$, this confirms zero steady-state error, no gain peaking in the complementary path.

Regarding the channel from load disturbance to output, the transfer functions can be derived from (14), which is

$$G_{\text{do}}(z) = \frac{U_o^a(z)}{I_{\text{load}}(z)} = \frac{T_s}{C_o}\frac{1 - z^{-1}}{z^2}. \tag{17}$$

This indicates that G_{do} has a zero at $z = 1$, and has two poles at $z = 0$, which means its a pure two-sample delay without gain peaking, and its sensitivity to constant/slow-varying loads is zero, with no steady-state errors.

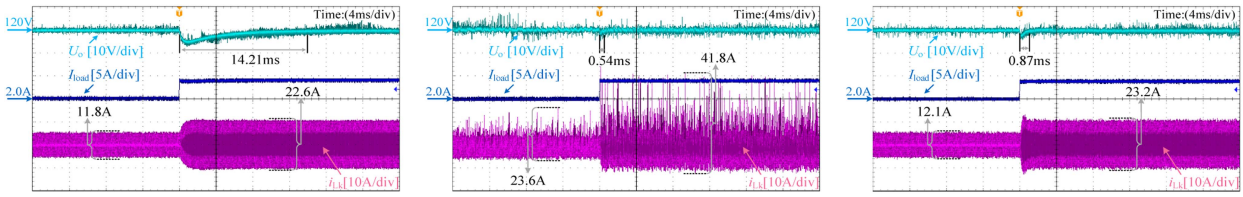

Fig. 7. Load step with synthetic sampling noise $\sigma = 0.2$. (a) PI controller. (b) Conventional deadbeat control method. (c) Proposed method.

Then, by using $z = e^{j\omega}$, $|G_{\mathrm{do}}(e^{j\omega})| = \frac{T_\mathrm{s}}{C_\mathrm{o}}|1 - e^{-j\omega}| = \frac{T_\mathrm{s}}{C_\mathrm{o}} 2\sin\frac{\omega}{2}$ can be obtained. The curve is also drawn in Fig. 4, with several information as follows.

1) $\lim_{\omega\to 0} |G_{\mathrm{do}}(e^{j\omega})| = 0$, which has similar characteristic as $S(e^{j\omega})$.

2) $\max_\omega |G_{\mathrm{do}}(e^{j\omega})| = 2T_\mathrm{s}/C_\mathrm{o}$, which means the worst-case (H_∞) gain is constrained by $2T_\mathrm{s}/C_\mathrm{o}$.

Consequently, benefiting from the two-sample pure-delay complementary sensitivity, the proposed method achieves unit-gain tracking and zero steady-state error, while constraining the impact of load disturbances with a tunable full-band bound. Thus, it can be seen that the proposed method preserves the characteristics of deadbeat control.

For the noises, the difference between (6) and the ideal output current without sampling noises is defined, serving to validate the noise-suppression capability. As shown in Fig. 5, with $\alpha \in [0, 1]$ and $\sigma \in [0, 0.7]$ (noises from 0 to 2.1 V), the proposed method demonstrates an excellent performance.

Therefore, it is shown that the proposed method enhances noise immunity without compromising the original dynamic optimality of the deadbeat response.

IV. Experiments Results

A DAB prototype is built to verify the proposed method, as shown in Fig. 6. Table I lists the parameters.

The performance of the proposed method is experimentally compared with the proportional-integral (PI) controller and the conventional deadbeat control. All experiments are conducted with the inherent sampling noises (around 0.2 V) from the real sampling system, and with the synthetic sampling noises that are emulated and injected by the microcontroller.

For the PI controller, the parameters are calculated according to [17], and are undergone trial and error process, especially considering the synthetic sampling noise. Therefore, $K_\mathrm{p} = 0.03$ and $K_\mathrm{i} = 80$. For the proposed method, the parameters $\beta = 0.1$, $\alpha_{\min} = 0.05$, and $\gamma = 60$ are set, according to the discussion in Section III-A.

First, the load-step tests are conducted with the synthetic sampling noises $\sigma = 0.2$ (99.7% noises are located within ± 0.6 V) and the inherent sampling noises (± 0.2 V). As shown in Fig. 7(a), the PI controller is hardly impacted by the noises, where the peak-to-peak transformer current stays around 11.8 and 22.6 A before and after the load step, respectively. However, it costs 14.21 ms to be recovered. The conventional deadbeat control, as shown in Fig. 7(b), achieves a much faster response speed (0.54 ms). Nevertheless, this outcome is unsatisfactory, as the plant suffers from significant chattering, resulting in 23.6 and 41.8 A peak-to-peak transformer current before and after load step, respectively, with noticeable voltage fluctuations on the output capacitor. In addition, the excessively fast transient response is attributed to the surge current at the instant of the load step. Fig. 7(c) illustrates results of the proposed method. As shown, it realizes a fast dynamic performance (0.87 ms), with a well-maintained peak-to-peak current (12.1 and 23.2 A) under noise conditions. It attains a high robustness for sampling noise while hardly affecting the high response speed of deadbeat control.

Next, along with the inherent sampling noise, the synthetic sampling noise changes from $\sigma = 0.2$ to $\sigma = 0.4$ (99.7% noises are located within ± 1.2 V). As shown in Fig. 8, the conventional deadbeat control is obviously impacted by the sampling noise, leading to dangerous current stress and chattering. Conversely, due to the adaptive attenuation coefficient, the proposed method can adapt various sampling noise, maintaining the system stability under different conditions.

To further test the proposed method, a multilevel extended-state observer (ESO) is employed as the comparative method [18]. In comparison to the conventional ESO, it achieves an enhanced resistance ability against sampling noises. The parameters are tuned to achieve the similar effect as the proposed method does.

As Fig. 9(a) shows, the multilevel ESO realizes a similar noise resistance ability (12.1 and 23.5 A), while inducing a much slower dynamic speed (7.74 ms) as a tradeoff. Fig. 9(b) shows the adaptive ability against the various sampling noise. It is evident that, in the absence of noise adaptivity, the chattering increases with the noise level (12.1 and 12.5 A). Therefore, compared with mainstream noise-suppression approaches, such as the multilayer ESO, the proposed method retains advantages in noise-suppression capability, dynamic response speed, and adaptivity.

Lastly, an experiment of input-voltage step with synthetic sampling noise $\sigma = 0.6$ (99.7% noises are located within ± 1.8 V) is also conducted.

As shown in Fig. 10, after the step, it produces an almost seamless output transient, exhibiting negligible overshoot/undershoot and no discernible settling delay. This is because, within the control loop of the DAB converter, the input voltage effectively enters only as a gain term. Unlike an output-voltage transient—which induces an instantaneous power mismatch and thus a large disturbance—variations in this gain have a much smaller impact on the control system.

Moreover, Fig. 10 illustrates the effect of sampling noise on the input voltage. Its influence on the final control performance is clearly much smaller than that of the output-voltage noise.

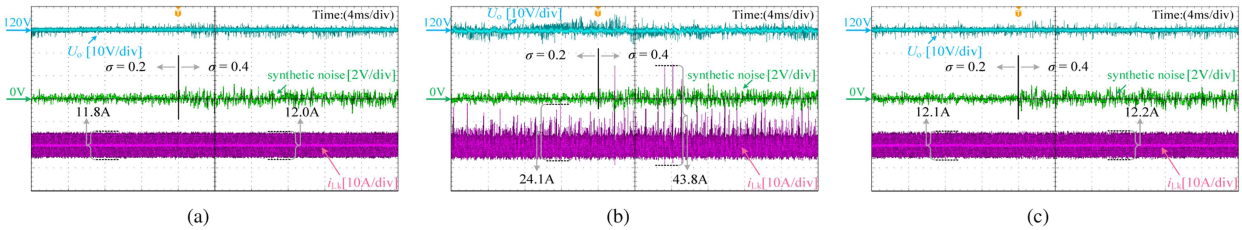

(a) (b) (c)

Fig. 8. Various synthetic sampling noise from $\sigma = 0.2$ to $\sigma = 0.4$. (a) PI controller. (b) Conventional deadbeat control method. (c) Proposed method.

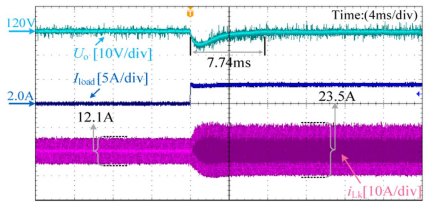

(a)

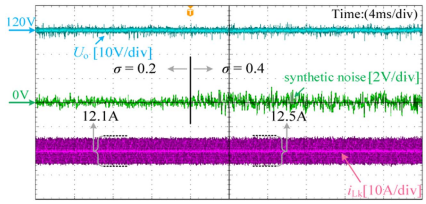

(b)

Fig. 9. Multilayer ESO with parameters for same noise resistance ability as the proposed method. (a) Load step. (b) Noise step from $\sigma = 0.2$ to $\sigma = 0.4$.

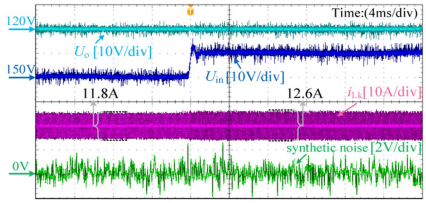

Fig. 10. Input-voltage step with synthetic sampling noise $\sigma = 0.6$ of the proposed method.

The increased transformer current stress after the input-voltage step is because the voltage gain changes. This experimental observation corroborates the analysis in Section II-B.

V. Conclusion

This letter proposes a method for deadbeat-controlled DABs to enhance adaptive noise resistance. Instead of using digital filters, the proposed method adopts an adaptive attenuation coefficient combined with a related compensation term. This approach achieves high robustness to sampling noise while preserving the fundamental characteristics and performance of deadbeat control. The mechanism and impact of sampling noise are analyzed, followed by a detailed description of the proposed method. System-level analysis theoretically validates its effectiveness, and experimental results further demonstrate the method's high robustness and fast dynamic response.

References

[1] S. Shao et al., "Modeling and advanced control of dual-active-bridge DC–DC converters: A review," *IEEE Trans. Power Electron.*, vol. 37, no. 2, pp. 1524–1547, Feb. 2022.

[2] Y. Sun, J. Zhu, C. Fu, and Z. Chen, "Decoupling control of cascaded power electronic transformer based on feedback exact linearization," *IEEE Trans. Emerg. Sel. Topics Power Electron.*, vol. 10, no. 4, pp. 3662–3676, Aug. 2022.

[3] N. Tiwary, V. Naik N, A. K. Panda, A. Narendra, and R. K. Lenka, "A robust voltage control of dab converter with super-twisting sliding mode approach," *IEEE J. Emerg. Sel. Topics Ind. Electron.*, vol. 4, no. 1, pp. 288–298, Jan. 2023.

[4] Y.-C. Jeung and D.-C. Lee, "Voltage and current regulations of bidirectional isolated dual-active-bridge DC–DC converters based on a double-integral sliding mode control," *IEEE Trans. Power Electron.*, vol. 34, no. 7, pp. 6937–6946, Jul. 2019.

[5] Q. Xiao, L. Chen, H. Jia, P. W. Wheeler, and T. Dragičević, "Model predictive control for dual active bridge in naval dc microgrids supplying pulsed power loads featuring fast transition and online transformer current minimization," *IEEE Trans. Ind. Electron.*, vol. 67, no. 6, pp. 5197–5203, Jun. 2020.

[6] L. Chen et al., "Moving discretized control set model-predictive control for dual-active bridge with the triple-phase shift," *IEEE Trans. Power Electron.*, vol. 35, no. 8, pp. 8624–8637, Aug. 2020.

[7] S. Li, Y. Xu, W. Zhang, and J. Zou, "Robust deadbeat predictive direct speed control for PMSM with dual second-order sliding-mode disturbance observers and sensitivity analysis," *IEEE Trans. Power Electron.*, vol. 38, no. 7, pp. 8310–8326, Jul. 2023.

[8] A. V. Peterchev and S. R. Sanders, "Quantization resolution and limit cycling in digitally controlled PWM converters," *IEEE Trans. Power Electron.*, vol. 18, no. 1, pp. 301–308, Jan. 2003.

[9] S. W. Smith, "The scientist and engineer's guide to digital signal processing," 1st ed. California Tech. Publishing, San Diego, CA, USA, Jan. 1997.

[10] I. Z. Petric, P. Mattavelli, and S. Buso, "Feedback noise propagation in multisampled DC–DC power electronic converters," *IEEE Trans. Power Electron.*, vol. 37, no. 1, pp. 150–161, Jan. 2022.

[11] K. Hasan, M. M. Othman, S. T. Meraj, S. Mekhilef, and A. F. B. Abidin, "Shunt active power filter based on Savitzky-Golay filter: Pragmatic modelling and performance validation," *IEEE Trans. Power Electron.*, vol. 38, no. 7, pp. 8838–8850, Jul. 2023.

[12] Y. He et al., "Direct predictive voltage control for grid-connected permanent magnet synchronous generator system," *IEEE Trans. Ind. Electron.*, vol. 70, no. 11, pp. 10860–10870, Nov. 2023.

[13] N. Agrawal, A. Kumar, V. Bajaj, and G. K. Singh, "Design of bandpass and bandstop infinite impulse response filters using fractional derivative," *IEEE Trans. Ind. Electron.*, vol. 66, no. 2, pp. 1285–1295, Feb. 2019.

[14] H. Peng, A. Prodic, E. Alarcón, and D. Maksimovic, "Modeling of quantization effects in digitally controlled DC–DC converters," *IEEE Trans. Power Electron.*, vol. 22, no. 1, pp. 208–215, Jan. 2007.

[15] A. Sangswang, "An experimental study of random noise characteristics in a power converter," in *Proc. IEEE Region 10 Conf.*, 2005, pp. 1–5.

[16] R. Dorf and R. Bishop, *Modern Control Systems*, 13th ed. Boston, MA, USA: Pearson, 2016.

[17] K. J. Astrom, *Pid Controllers: Theory, Design, and Tuning*. Durham, NC, USA: ISA—Instrum., Syst. Autom. Soc., 1995.

[18] O. Babayomi, J. Kim, and K.-B. Park, "Disturbance observer-based control with sensor noise suppression for dab converters," in *Proc. IEEE Energy Convers. Congr. Expo.*, 2024, pp. 3854–3856.